Epilepsia, **47**(1):134–142, 2006
Blackwell Publishing, Inc.

In Vivo Profiling of Focal Cortical Dysplasia on High-resolution MRI with Computational Models

Olivier Colliot, Samson B. Antel, Veronique B. Naessens, Neda Bernasconi, and Andrea Bernasconi

Department of Neurology and Neurosurgery and McConnell Brain Imaging Center, Montreal Neurological Institute, McGill University, Montreal, Quebec, Canada

Summary: *Purpose:* On MRI, focal cortical dysplasia (FCD) is characterized by a combination of increased cortical thickness, hyperintense signal within the dysplastic lesion, and blurred transition between gray and white matter (GM–WM). The visual identification of these abnormal characteristics may be difficult, and it is unclear to what degree these features occur among different FCD lesions. Our purpose was to investigate the pattern of occurrence of abnormal MRI characteristics in FCD by using a set of computational models and to generate quantitative lesion profiling.

Methods: A set of voxel-wise operators was applied to high-resolution 3D T_1-weighted MRI in 23 patients with histologically proven FCD and 39 healthy controls, creating maps of GM thickness, maps of relative intensity highlighting areas with hyperintense signal, and maps of gradient magnitude modeling the GM–WM transition. All FCD lesions were segmented manually on the T_1-weighted MRI.

Results: FCD volumes ranged from 734 mm^3 to 80,726 mm^3 (mean, 8,629 mm^3 $\pm$ 16,238). The manually segmented FCD lesions were used to estimate features in the lesional area and to determine possible local variations of each feature by means of a histogram. In 78% of the patients, FCD lesions were characterized by simultaneous GM thickening, hyperintense signal, and blurring of the GM–WM transition. Moreover, in all patients, the FCD lesion had at least two of these three characteristics.

Conclusions: The three features occurred regardless of the lesion volume, and they characterized not only large FCD lesions, but also subtle ones that had been overlooked by conventional radiologic inspection before surgery. **Key Words:** Magnetic resonance imaging—Image analysis—Focal cortical dysplasia.

Malformations caused by abnormalities of cortical development have been increasingly recognized in patients with drug-resistant epilepsy. Focal cortical dysplasia (FCD) (1), the most common malformation of cortical development in surgical reports (2,3), is characterized by a spectrum of histopathologic abnormalities that include various degrees of focal cortical thickening, blurring of the gray matter (GM)–white matter (WM) transition, abnormal neuroglial elements in the underlying WM, and disruption of the normal cortical lamination associated with an excess of large aberrant neurons and balloon cells in most of the cases (1,4,5).

The use of magnetic resonance imaging (MRI) has allowed the identification of FCD in an increasing number of patients. On T_1-weighted MRI, FCD may demonstrate focal GM thickening (6) and a blurred GM–WM transition (6,7). More rarely, hyperintense signal within the dysplastic lesion relative to normal cortex has been described (8–10). Hyperintense signal within the FCD lesion is often not visible on the T_1-weighted MRI because it is subtle and at times limited to a portion of the FCD lesion. However, signal-intensity differences between the lesion and the normal cortical GM can be measured from the T_1-weighted MRI (9).

In previous qualitative MRI studies, cortical thickening and abnormalities in the GM–WM transition have been reported in isolated FCD cases (11–16). These reports have been focused on the presence (or absence) of abnormalities among FCD lesions and have not addressed the question of their severity in individual patients. Moreover, the visual identification of these abnormal tissue characteristics on MRI is sometimes difficult and may be subjective, relying on assessment by trained observers.

Processing of MR images allows generation of 3D maps and quantitative measurements that are reproducible and rater independent. A common goal of processing techniques applied to neuroimaging is to improve detection of abnormal brain tissue, including abnormalities that may not be readily recognizable by visual analysis alone. We previously developed image-processing operators modeling FCD characteristics as seen on T_1-weighted high-resolution MRI: GM thickening, hyperintense signal

Accepted July 4, 2005.
Address correspondence and reprint requests to Dr. A. Bernasconi at Montreal Neurological Hospital and Institute, 3801 University Street, Montreal, Quebec, Canada H3A 2B4. E-mail: andrea@bic.mni.mcgill.ca

within the dysplastic lesion, and blurring of the GM–WM transition (9,17,18). We demonstrated that these computational models significantly improve the sensitivity of visual detection of FCD lesion relative to standard MRI evaluation (9). In our previous analysis, the identification of FCD lesions relied on a ratio map combining the three models of these characteristics in a single numeric value. Therefore we did not examine separately the occurrence of each characteristic. For example, it is unclear whether all FCD lesions present the three MRI abnormalities simultaneously or only one or two of them. It also is unknown whether large and small FCD lesions share the same abnormal tissue characteristics. Moreover, even though it is known that abnormal tissue characteristics in FCD may vary across patients, no systematic and quantitative study has been undertaken of the degree of such changes in individual patients.

The purpose of our study was to assess quantitatively abnormal MRI characteristics in FCD by using computational models of GM thickness, tissue hyperintensity, and blurring of the GM–WM transition, and to investigate the pattern of occurrence of these abnormalities among FCD lesions.

METHODS

Subjects

We selected 23 patients [12 males; mean age ± standard deviation (SD), 23 ± 9.2 years] who had histologically proven FCD at operation and who had preoperative high-resolution 3D T_1-weighted MRI. Patients were compared with 39 sex- and age-matched healthy controls (17 males; mean age, 28 ± 8.4). The Ethics Board of the Montreal Neurological Institute and Hospital approved the study, and written informed consent was obtained from all participants.

All patients underwent a comprehensive evaluation including prolonged video-EEG monitoring. The seizure focus was right-sided in 15 patients and left-sided in eight. Eleven patients had frontal lobe epilepsy; in five patients, the seizure focus was parietal, in six, central, and in one, occipital.

Resections were carried out in the frontal lobe in 11 patients, the central area in six patients, the parietal lobe in five, and the occipital lobe in one. Qualitative histologic classification of the resected tissue was done according to the grades proposed by Palmini et al. (5). In this classification, grade IA is characterized by isolated architectural abnormalities; grade IB is an association of architectural abnormalities and giant or immature but not dysmorphic neurons; grade IIA consists of architectural abnormalities with dysmorphic neurons but without balloon cells; and grade IIB is composed of architectural abnormalities with dysmorphic neurons and balloon cells. According to this classification, 15 of our patients had FCD grade IIB, five had FCD grade IIA, and three had FCD grade IB.

MRI acquisition

In all subjects, MR volumetric images were acquired on a 1.5-T Gyroscan (Philips Medical System, Best, The Netherlands) by using a T_1-fast field echo sequence (TR, 18; TE, 10; one acquisition average pulse sequence; flip angle, 30 degrees; matrix size, 256 × 256; FOV, 256; thickness, 1 mm). This high-resolution T_1-weighted 3D gradient-echo sequence was chosen because it provides exquisite anatomic details with an isotropic voxel size of 1 × 1 × 1 mm. This acquisition type also features high signal-to-noise and contrast-to-noise (17). As part of our clinical protocol, coronal and axial proton-density (PD) and T_2-weighted images (thickness, 3.0–5.0 mm; gap, 0.3; TR, 2,100 ms; TE, 20, 78 ms) were obtained in all patients and showed an increase in signal within the lesion in 14 of them. Coronal fluid attenuation inversion recovery images (FLAIR; slice thickness, 3.0 mm; interslice gap, 0.3 mm; TR, 6,000 ms; TE, 150 ms; TI, 1,900 ms; FOV, 230 mm) were obtained in 14 patients and showed signal abnormality in five of them.

Based on this protocol, the FCD lesion was recognized before surgery in 16 patients. In the remaining seven patients, the lesion was not seen by using the clinical MR protocol that consisted of T_1-weighted, PD, and T_2-weighted images (in all seven patients) and FLAIR (in four of seven patients). In these patients, surgery was based on strong clinical and EEG colocalizing data. The subtle FCD lesion was retrospectively recognized after surgery by performing curvilinear reformatting of 3D preoperative T_1-weighted MRI (19).

Image preparation

Images were automatically registered into stereotaxic space to adjust for differences in total brain volume and brain orientation (20). Each image underwent automated correction for intensity nonuniformity and intensity standardization (21). This correction produces consistent relative GM, WM, and cerebrospinal fluid (CSF) intensities. Classification of brain tissue into GM, WM, and CSF was done by using our previously implemented histogram-based method with automated threshold (17).

Computational models of FCD

To model cortical thickness, blurring of the GM–WM transition and hyperintense signal, a set of voxel-wise operators was applied to the high-resolution T_1-weighted MRI for each subject by using our previously developed methods (9,17) that generate a quantitative 3D map of each feature. An example in an individual FCD patient is shown in Fig. 1.

Cortical thickness was measured by modeling the cortex as an electrostatic field as described by Jones et al. (22). In brief, borrowing a tool from mathematical physics, Laplace's equation is solved over the cortical volume with boundary conditions specified at the GM–WM and GM–CSF transitions, creating a series of streamlines

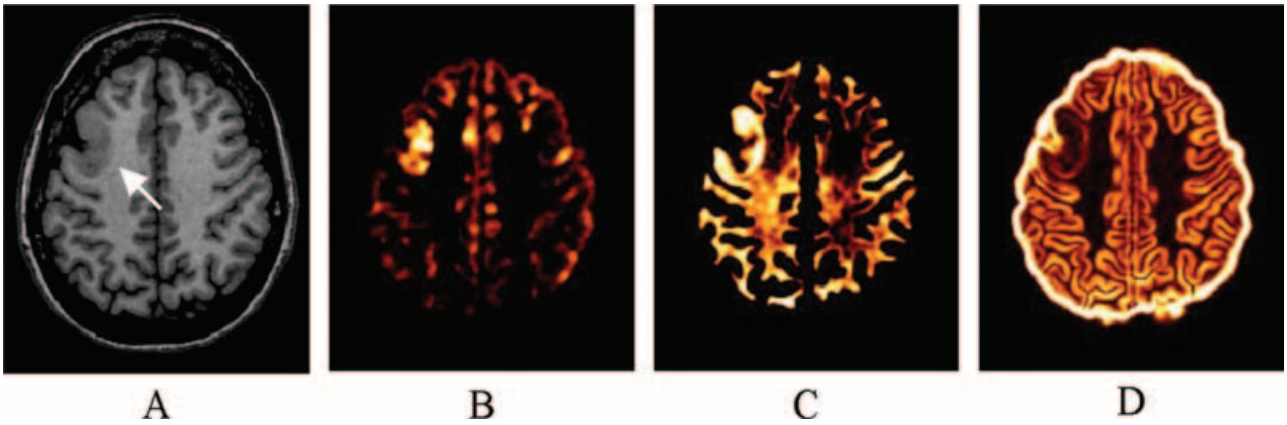

FIG. 1. Computational models of MRI characteristics of focal cortical dysplasia (FCD). For each feature, a three-dimensional map is created. Representative axial slices are shown. **A:** T_1-weighted MRI with frontal FCD (*arrow*). **B:** Cortical-thickness map; brighter values indicate higher thickness. **C:** Relative-intensity map; brighter values indicate hyperintense voxels. **D:** Gradient map; darker values indicate a blurred transition at the gray- and white-matter interface.

corresponding to "equipotential surfaces." Cortical thickness at a given voxel is then defined as the length of the path that connects the voxel to both the GM–WM and GM–CSF transitions and is orthogonal to all intermediary streamlines. On the cortical-thickness map, higher intensity corresponds to increased GM thickness (Fig. 1B).

To model the hyperintense signal within the FCD lesions, we calculated a feature denoted as relative intensity, defined for a particular voxel as

$$100 \times [Bg - |Bg - g(i, j, k)|]/Bg$$

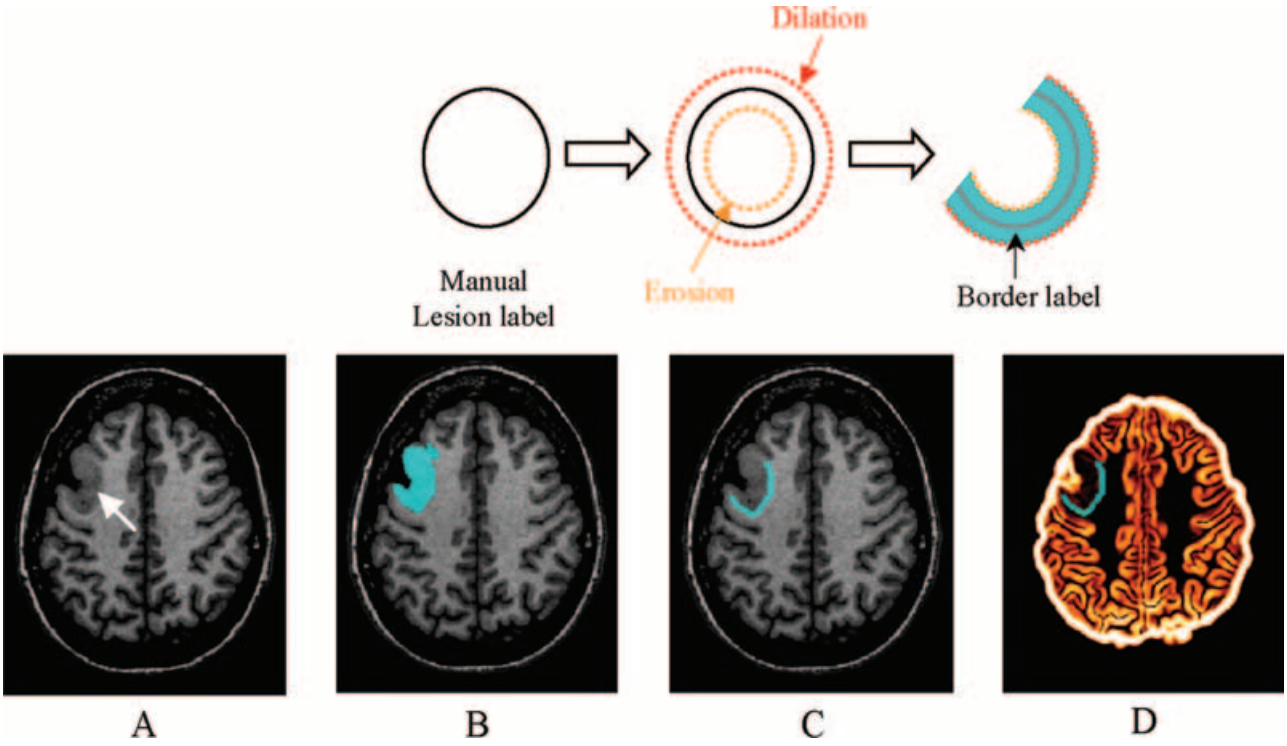

FIG. 2. Computational model of gray matter–white matter (GM–WM) blurring along the edges of focal cortical dysplasia FCD. **Upper panels:** The construction of a border label from the manually segmented FCD. First, a 2-mm dilation and a 2-mm erosion of the manually segmented lesion are computed. The 4-mm-wide border label is then obtained by subtracting the 2-mm erosion to the 2-mm dilation. **Lower panels:** An FCD lesion label and its border corresponding to the GM–WM interface. **A:** T_1-weighted MRI with frontal FCD (*arrow*). **B:** Manually segmented FCD. **C:** Area corresponding to the GM–WM transition on T_1-weighted MRI, excluding parts corresponding to the GM–CSF transition. **D:** Border label superimposed on the gradient map.

where Bg is the intensity at the boundary between GM and WM, and g(i, j, k) represents the intensity at the given voxel (9). Using the relative difference allows the analysis of voxels located within cortical GM in which the intensity is higher than normal and may even overlap that of the WM. On the relative-intensity map, higher intensity corresponds to hyperintense signal within the lesion (Fig. 1C).

Blurring of the GM–WM transition was modeled with a gradient magnitude map (17). In the MR image, highest gradient values are generated in regions of abrupt voxel-intensity changes, such as the transition between WM and GM or GM and CSF. In this 3D map, areas of blurred GM–WM transition have lower gradient values than areas of normal GM–WM transition (Fig. 1D).

FCD lesion profiling

Features computation in patients with FCD

To allow computation of each feature within the lesional tissue, FCD lesions were segmented manually on high-resolution T_1-weighted MRI by a trained rater (V.N.), with the MNI-Display software, which allows labeling in the three directions of space. In the seven patients in whom the FCD lesion had not been recognized by using the standard MR protocol, the lesion could be seen on the brain surface as obtained by curvilinear reformatting of 3D MRI with the in-house–developed software *Brainsight* (19). This software allows a simultaneous display of multiplanar and curvilinear slices, thus providing a direct correspondence between the two views. Once the location of the lesion was determined on the curvilinear slices, the FCD was segmented on the orthogonal MRI slices.

For each patient, we computed the mean thickness and relative intensity in the GM component of the FCD lesion, defined as the intersection of the lesion label and the GM segmentation.

The gradient was computed along the edges of the FCD lesion, at the GM–WM transition (Fig. 2). To this end, we subtracted a 2-mm erosion from a 2-mm dilation of the lesion label, producing a 4-mm-wide border label. This border label was subsequently manually corrected to include only the GM–WM transition (excluding parts corresponding to the GM–CSF transition) (Fig. 2C and D).

To analyze quantitatively the spatial distribution of FCD lesions, we constructed a statistical parametric anatomic map (SPAM) (Fig. 3). This SPAM, obtained by computing the addition of all lesion labels in all 23 patients, indicates the proportion of FCD lesions that were present at a given voxel.

Features computation in healthy controls

The computation of each feature in healthy controls was performed as described earlier only in brain areas corresponding to the distribution of FCD lesions in the patients as determined by the SPAM. To define our region of interest, we first drew a mask on an average template of 152 linearly registered healthy subjects. Then cortical thickness and relative intensity were computed in the GM part of the mask. The gradient was computed on a region corresponding to the GM–WM transition as defined by the 2-mm dilation of the intersection of two gaussian peaks fitted to GM and WM.

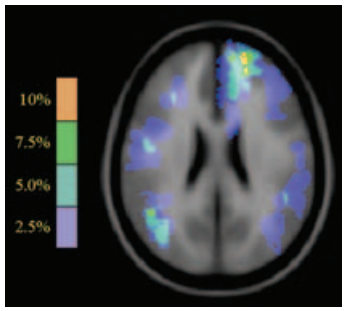

FIG. 3. Statistical parametric anatomic map (SPAM) of focal cortical dysplasia (FCD) distribution superimposed on the ICBM 152 average template of healthy control subjects. The color-coding indicates the proportion of lesions present in a given voxel.

Analysis

Numeric values

Group differences were assessed by using Student's *t* test. For analysis of individual patients, a given feature was considered abnormal if its value was 2 SD above or below the mean of healthy controls.

The degrees of abnormalities were assessed by subdividing the patients into three groups constructed by using intervals of equal width: 4–6 mm, 6–8 mm, and >8 mm for cortical thickness; 82–85, 85–88, and >88 (arbitrary units) for relative intensity; and 100–80, 80–60, and < 60 (arbitrary units) for gradient.

Associations between computational features and the FCD volume, as determined by manual segmentation, were assessed by using the Pearson correlation coefficient (r).

Histograms

To determine possible local variations of features throughout the FCD lesion, we calculated the histogram of each feature within the manually segmented lesion label. The normalized histogram is defined as a function *h* equal to the proportion of voxels in the lesion corresponding to each possible feature value. Formally,

$$h(x) = N_x/N$$

where N_x is the number of lesion voxels having a value equal to x, and N is the number of voxels in the lesion. For example, on Fig. 4A, in the thickness histogram, a value of 12% on the ordinate corresponding to 4 mm on the abscissa means that 12% of the voxels of the lesion have a thickness value equal to 4 mm. The normalization

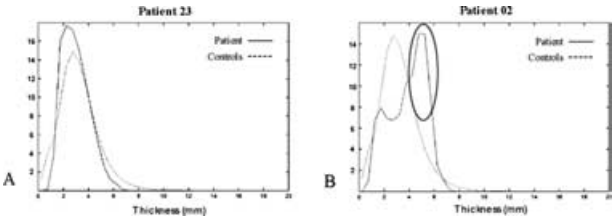

FIG. 4. Examples of histograms of cortical thickness in two patients with normal mean (numeric) values. The histogram of each patient (*continuous line*) is superimposed on the mean histogram corresponding to the healthy controls (*dashed line*). Details concerning histogram construction are given in the text. **A:** The almost identical graphs indicate that the focal cortical dysplasia (FCD) does not exhibit any area of increased gray matter (GM) thickness. **B:** The lesion has an area of GM thickening (revealed by the *oval* on the histogram). The normal mean thickness value of this patient is explained by the fact that higher values are counterbalanced by a substantial number of low thickness values.

makes the histogram independent of the lesion size and makes it possible to compare histograms across subjects.

We also computed the histogram of each control subject in a similar manner. We then computed the mean histogram h from the histograms $h_1, \ldots, h_{39}$ of all 39 healthy controls:

$$h(x) = (h_1 + h_2 + \ldots + h39)/39.$$

To assess the local abnormalities in a given patient, we superimposed its histogram on the mean histogram of controls. Whenever the patient has a higher histogram value than the control histogram, it means that it has a higher percentage of voxels with that feature value than do normal subjects. Two examples of patients' histograms superimposed on the control histogram are shown in Fig. 4.

RESULTS

Group analysis

Descriptive statistics for each feature in healthy controls and FCD patients are presented in Table 1. For controls, the coefficient of variability was 13% for cortical thickness, 2% for relative intensity, and 5% for gradient.

Mean thickness in the GM component of the FCD lesion was higher in patients than in the corresponding GM area in healthy controls (6.5 mm vs. 3.2 mm; $p < 0.001$). The mean relative intensity of the MR signal within the FCD lesions also was higher than that of the corresponding GM in controls (84.9 vs. 79.4; $p < 0.001$). The gradient was lower (73.3 vs. 112.9; $p < 0.001$), indicating a significant blurring of the GM–WM transition along the edges of the FCD lesion.

FCD lesions volumes ranged from 734 mm^3 to 80,726 mm^3 (mean, 8,629 $mm^3 \pm 16{,}238$). No correlation was found between FCD volume and cortical thickness, relative intensity, and blurring of the GM–WM transition along the edges of the FCD lesion.

In the seven patients in whom the FCD had not been detected before surgery, the mean thickness was higher than that in the corresponding GM areas of controls (5.6 mm vs. 3.2 mm; $p < 0.001$). The mean relative intensity was also higher than that of controls (85.4 vs. 79.4; $p < 0.005$), and the gradient was lower (81.3 vs. 112.9; $p < 0.005$). Compared with the 16 patients in whom the FCD had been recognized on the preoperative MRI, these seven patients had smaller lesions (1,610 mm3 vs. 11,700 mm3; $p < 0.05$) and exhibited lower cortical thickness (5.6 mm vs. 7.0 mm; $p < 0.05$). However, they did not differ in terms of relative intensity (85.4 vs. 84.6; $p = 0.56$) or blurring of the GM–WM transition (81.3 vs. 69.8; $p = 0.20$).

When comparing feature values of FCD lesions with balloon cells to those without balloon cells, we found no differences in the mean cortical thickness (7 mm vs. 5.7 mm), relative intensity (85.2 vs. 84.3), and blurring of the GM–WM transition along the edges of the FCD lesion (72 vs.76).

Individual analysis

The ranges of feature values across FCD lesions are presented in Fig. 5 and Table 2. Twenty-one (91%) patients exhibited an increased cortical thickness, 20 (87%), an abnormal relative intensity, and 22 (96%), a blurring of the GM–WM transition. Table 2 shows the distribution of abnormalities across patients. Eighteen (78%) patients had all three features abnormal, four (17%) had two abnormal features (two patients, cortical thickening and blurring; one, hyperintensity and blurring; one, cortical thickening and hyperintensity), and one (4%) had only one abnormal feature (which was a blurring). No patient had all three features normal.

TABLE 1. *Descriptives for cortical thickness, tissue relative intensity, and blurring of the GM–WM transition for healthy controls (n = 39) and patients with FCD (n = 23)*

	Cortical thickness (mm)	Relative intensity (arbitrary units)	Gradient (arbitrary units)
Controls	3.2 ± 0.4 (2.4–4.0)	79.4 ± 1.3 (76.8–82.6)	112.9 ± 5.8 (100.2–127)
FCD patients	6.5 ± 1.9 (2.7–10.2)	84.9 ± 3.0 (78.6–90.2)	73.3 ± 17.1 (42.8–115.5)

Each cell of the table displays the mean ± SD and the range in brackets.
FCD, focal cortical dysplasia; GM, gray matter; WM, white matter.

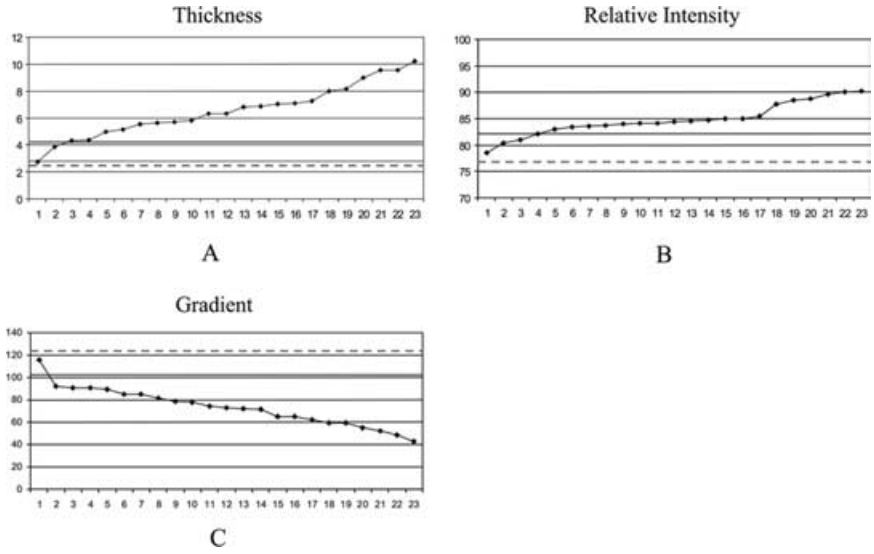

FIG. 5. Range of variation for **(A)** cortical thickness, **(B)** relative intensity, and **(C)** gradient in focal cortical dysplasia. The X-axis corresponds to the 23 patients. The Y-axis represents the values of cortical thickness (in millimeters), relative intensity, and gradient (arbitrary units). The two *horizontal lines* indicate the interval mean (*dashed line*) ±SD (*continuous line*) corresponding to the values found in the healthy controls.

The histogram analysis showed that one of the two patients with normal mean thickness had a portion of the lesion with abnormal cortical thickening (see Fig. 4). In the three patients with normal relative intensity as well as in the patient with normal gradient, histogram analysis revealed no focal area of abnormality within the FCD. Adding these cases to the analysis, the proportion of patients with abnormal thickening in the GM component of the FCD lesion increased to 96% (22 of 23). The proportion of patients with two abnormal features increased to 22% (five of 23).

Table 3 presents feature values and lesion size corresponding to the seven patients whose conventional MRI was considered normal before surgery. Representative examples of the various feature patterns, including FCD lesions with normal features and those with various degrees of abnormalities, are presented in Fig. 6. This figure includes images of patients whose MRIs had been reported as normal (panels A and B) as well as those of a patient whose lesions had been recognized before surgery (panel C).

DISCUSSION

By using a set of computational models, we were able to assess quantitatively the abnormal MRI characteristics of FCD lesions on high-resolution MRI and provide an objective evaluation of both the presence and degree of these abnormalities. Specifically, we could analyze intra- and interlesional variations of thickness and relative intensity in the GM component of the FCD lesion and blurring of the GM–WM transition along its edges.

Group analysis revealed that all three features were significantly different in the FCD lesions compared with topographically similar areas in healthy controls, indicating that these features discriminate FCD from normal brain tissue. The low interindividual variability of mean cortical thickness, GM intensity, and blurring of the GW–WM transition in healthy controls indicates the high reliability of our measurements and underlines their potential in distinguishing subtle changes along the continuum of disease severity.

The simultaneous presence of GM thickening, hyperintense signal within the FCD lesion, and blurring of the GM–WM transition characterized more than three fourths of the FCD lesions included in this study. Moreover, all FCD lesions were characterized by statistically significant changes in at least two features. Some FCD lesions were composed predominantly of voxels with normal feature values resulting in normal mean values for each characteristic, thus obscuring the relatively few abnormal

TABLE 2. *Degree of abnormality in cortical thickness, tissue relative intensity, and blurring of the GM–WM transition for FCD lesions*

	Cortical thickness (mm)		Relative intensity (arbitrary units)		Gradient (arbitrary units)	
Number of patients with normal values	2 (9%)		3 (13%)		1 (4%)	
Degree of abnormality	Interval	Patients	Interval	Patients	Interval	Patients
	4–6 mm	8 (35%)	82–85	12 (52%)	100–80	7 (30%)
	6–8 mm	7 (30%)	85–88	3 (13%)	80–60	9 (39%)
	>8mm	6 (26%)	>88	5 (22%)	< 60	6 (26%)

FCD, focal cortical dysplasia; GM, gray matter; WM, white matter.

TABLE 3. *Cortical thickness, relative intensity, and gradient in the seven patients whose conventional MRI had been reported as normal before surgery*

	Lesion size (mm^3)	Cortical thickness (mm)	Relative intensity (arbitrary units)	Gradient (arbitrary units)
Patient 02	734	**3.9** [a]	81.0	71.4
Patient 03	1559	5.7	84.5	**115.5**
Patient 04	807	6.8	90.0	55.0
Patient 06	773	5.5	83.7	89.6
Patient 08	3,093	5.0	85.5	90.7
Patient 09	2,460	6.9	88.4	74.1
Patient 19	1,850	5.1	85.0	73.0

Values falling in the range of healthy controls are indicated in **bold**.
[a]Subtle local abnormalities were revealed by the histogram analysis.

voxels. By using a complementary histogram-based analysis of the three features, we were able to uncover abnormalities, even though they were present in a minority of lesional voxels. Overall, we found that the most common abnormal MRI features of FCD were a blurring of the GM–WM transition along the edges of the lesion (present in 96% of lesions) and GM thickening (96%), followed by lesion hyperintensity (87%). The three features occurred regardless of the FCD volume, indicating that they characterize not only large lesions, but also very subtle ones.

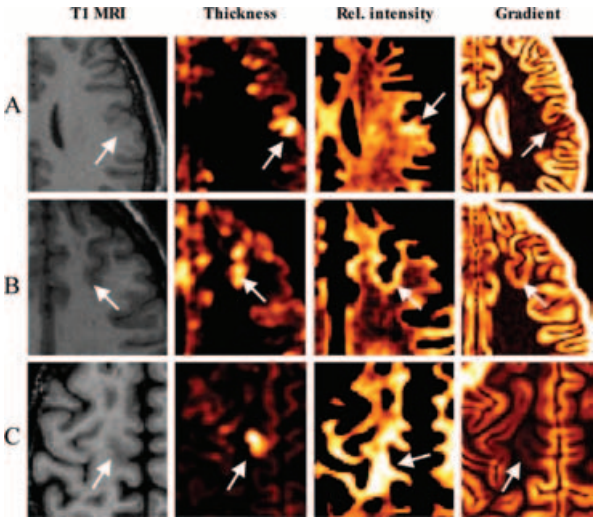

FIG. 6. Examples of different patterns of features profiles in focal cortical dysplasia lesions. MR images in patients A and B had been reported as normal before surgery. In patient C, the lesion had been recognized before surgery. For each lesion, a representative slice of the T_1-weighted MRI, the cortical-thickness map, the relative-intensity map, and the gradient map are shown from left to right. **A:** Patient 4, with dominant hyperintensity (90), high blurring (55), and medium cortical thickening (6.8 mm). **B:** Patient 3, with low cortical thickening (5.7 mm), low hyperintensity (84.5), and no blurring (115.5). **C:** Patient 10, with both dominant blurring (48) and hyperintensity (90.2) and low cortical thickening (5.8 mm). Numbers between brackets represent mean feature values.

The seven patients whose conventional MRIs were reported as normal before surgery had significantly smaller lesions. Even though these lesions were overlooked by visual inspection, our quantitative analysis demonstrated that they were characterized by increased GM thickness, signal hyperintensity, and blurring of the GM–WM transition, compared with healthy controls. This indicates that MRI abnormalities associated with subtle FCD lesions may be inaccessible to standard radiologic analysis mainly because of the size of the lesion rather than the absence of typical FCD characteristics. However, it should be noted that in three patients, the FLAIR sequence, which has been shown to be sensitive to subtle signal abnormalities associated with FCD (6), was not performed.

Although the vast majority of lesions are characterized by cortical thickening, signal hyperintensity, and blurring of the GM–WM transition, the individual analysis showed that a large variability exists in the degree of abnormalities across patients. Moreover, the histogram analysis revealed a substantial intralesional variability of the three features. A significant portion of lesional voxels may be characterized by normal feature values. We advocate that these findings should be taken into account when designing automated procedures for the identification of FCD lesions.

The inherent complexity of the brain's convolutional pattern makes the visual identification of MRI findings associated with subtle FCD a difficult task. The evaluation of the blurring of the GM–WM transition, usually done on low-resolution T_2-weighted MRIs, is very subjective, and signal intensity in the FCD lesion may be difficult to differentiate from the one of the surrounding GM (8,14,23). Previous MRI studies (12–16,24,25), based exclusively on qualitative examination of T_1-weighted MRI with thick partitioning and T_2-weighted images in a small number of adult patients, reported a wide range of abnormalities. Focal GM thickening was described in 45–100% of the patients. Blurring of the GM–WM transition and hyperintense T_2-weighted signal within the lesion were evaluated only in some studies and were reported in 30–100% of cases. To our knowledge, this is the first study providing quantitative in vivo profiles of FCD tissue characteristics. Compared with other studies, our approach to FCD lesion profiling presents several advantages. Computational models operate in 3D and allow the simultaneous analysis of consecutive MR sections, whereas a human observer performing standard visual analysis examines the brain volume a slice at a time, and therefore must mentally synthesize information from consecutive slices. Furthermore, our method provides an automatic and objective evaluation of MRI characteristics of FCD in a large series of patients and a reliable comparison with healthy controls. Because our analysis is based on high-resolution 3D T_1-weighted MRI, we were able to provide a very sensitive measurement of the different degrees of abnormalities. In addition, the histogram analysis allowed the

detection of local feature differences that remained undetected by the global numeric analysis over the entire lesion.

The in vivo MRI identification of subtypes of FCD may be clinically relevant, in particular with respect to surgical planning. Some studies indicate that different FCD types may be differently related to ictal generation and preservation of function (16,26,27). A recent report suggested that FCD lesions without balloon cells harbor the ictal-onset zone and retain motor function, in contrast to those with balloon cells, which are functionally silent and not associated with seizure onset (28). When comparing features values of FCD lesions with and those without balloon cells, we found no significant differences in the mean cortical thickness, relative intensity, and blurring of the GM–WM transition along the edges of the lesion. Therefore in our patients, MRI signal alterations were not sufficiently different to allow in vivo discrimination between the two types of FCD. It should nevertheless be noted that the group without balloon cells included only eight patients.

To date, information about the location of the FCD lesions has been based on qualitative assessment done by visual inspection of MR images. The analysis of several studies indicates that Taylor-type FCD is typically found in extratemporal areas and frequently involves either the frontal lobe only, the frontocentral, the perirolandic areas, or the posterior quadrant (12–15,29). Using lesion labeling and statistical parametric anatomic maps, we were able to demonstrate that, although FCD lesions were diffusely distributed within cerebral hemispheres, they predominated in the frontal lobe. In particular, they were more frequent in the mesial aspect of right frontobasal area (see Fig. 3). However, this finding must be confirmed in a larger series.

In our previous publications, we demonstrated the clinical utility of quantitative analysis of FCD characteristics by showing a significant increase in the FCD detection rate compared with conventional MR analysis (9,18). In this study, by using our quantitative profiling based on computational models of FCD, we demonstrated that the majority of FCD lesions are characterized by the simultaneous presence of various degrees of blurring of the GM–WM transition, GM thickening, and hyperintense signal within the lesion. These features characterize not only large FCD lesions but also those that could be easily overlooked on conventional MRI visual examination because of their small size. Furthermore, the individual analysis revealed large inter- and intralesional variability in the degrees of abnormalities. We believe that this new finding is relevant for clinical practice because it could influence the way that clinicians evaluate the MRI visually in patients in whom FCD is the suspected cause for intractable seizures. Furthermore, the information provided by the in vivo profiling of FCD has the potential to improve the sensitivity of existing tools for automatic detection of FCD (18). It is hoped that, in the near future, these techniques will be integrated in the routine clinical evaluation of patients who are candidates for epilepsy surgery.

Acknowledgments: This work was supported by a grant of the Canadian Institutes of Health Research (CIHR) and by the Scottish Rite Charitable Foundation of Canada. O.C. is recipient of the Epilepsy Canada Clinical Sciences Fellowship. The authors are grateful to Dr F. Andermann and F. Dubeau for referring patients to the study, Drs. D. Tampieri and D. Melanson for their reviews of the clinical MRI data, and Dr J. Richardson for the review of pathological specimens.

REFERENCES

1. Taylor DC, Falconer MA, Bruton CJ, et al. Focal dysplasia of the cerebral cortex in epilepsy. *J Neurol Neurosurg Psychiatry* 1971;34:369–387.
2. Sisodiya SM. Surgery for malformations of cortical development causing epilepsy. *Brain* 2000;123:1075–1091.
3. Frater JL, Prayson RA, Morris IH, et al. Surgical pathologic findings of extratemporal-based intractable epilepsy: a study of 133 consecutive resections. *Arch Pathol Lab Med* 2000;124:545–549.
4. Prayson RA, Spreafico R, Vinters HV. Pathologic characteristics of the cortical dysplasias. *Neurosurg Clin North Am* 2002;13:17–25.
5. Palmini A, Najm I, Avanzini G, et al. Terminology and classification of the cortical dysplasias. *Neurology* 2004;62:S2–S8.
6. Barkovich AJ, Raybaud CA. Malformations of cortical development. *Neuroimaging Clin North Am* 2004;14:401–423.
7. Bernasconi A. Quantitative MR imaging of the neocortex. *Neuroimaging Clin North Am* 2004;14:425–436.
8. Mackay MT, Becker LE, Chuang SH, et al. Malformations of cortical development with balloon cells: clinical and radiologic correlates. *Neurology* 2003;60:580–587.
9. Bernasconi A, Antel SB, Collins DL, et al. Texture analysis and morphological processing of magnetic resonance imaging assist detection of focal cortical dysplasia in extra-temporal partial epilepsy. *Ann Neurol* 2001;49:770–775.
10. Kirchhof K, Harting I, Bast T, et al. [Focal cortical dysplasias: neuroradiological findings and differential diagnosis]. *Rofo* 2003;175:1056–1063.
11. Gomez-Anson B, Thom M, Moran N, et al. Imaging and radiological-pathological correlation in histologically proven cases of focal cortical dysplasia and other glial and neuronoglial malformative lesions in adults. *Neuroradiology.* 2000;42:157–167.
12. Usui N, Matsuda K, Mihara T, et al. MRI of cortical dysplasia: correlation with pathological findings. *Neuroradiology* 2001;43:830–837.
13. Bronen RA, Vives KP, Kim JH, et al. Focal cortical dysplasia of Taylor, balloon cell subtype: MR differentiation from low-grade tumors. *AJNR Am J Neuroradiol* 1997;18:1141–1151.
14. Urbach H, Scheffler B, Heinrichsmeier T, et al. Focal cortical dysplasia of Taylor's balloon cell type: a clinicopathological entity with characteristic neuroimaging and histopathological features, and favorable postsurgical outcome. *Epilepsia* 2002;43:33–40.
15. Matsuda K, Mihara T, Tottori T, et al. Neuroradiologic findings in focal cortical dysplasia: histologic correlation with surgically resected specimens. *Epilepsia* 2001;42(suppl 6):29–36.
16. Tassi L, Colombo N, Garbelli R, et al. Focal cortical dysplasia: neuropathological subtypes, EEG, neuroimaging and surgical outcome. *Brain* 2002;125:1719–1732.
17. Antel SB, Bernasconi A, Bernasconi N, et al. Computational models of MRI characteristics of focal cortical dysplasia improve lesion detection. *Neuroimage* 2002;17:1755–1760.
18. Antel SB, Collins DL, Bernasconi N, et al. Automated detection of focal cortical dysplasia lesions using computational models of their MRI characteristics and texture analysis. *Neuroimage* 2003;19:1748–1759.

19. Bastos AC, Comeau RM, Andermann F, et al. Diagnosis of subtle focal dysplastic lesions: curvilinear reformatting from three-dimensional magnetic resonance imaging. *Ann Neurol* 1999;46:88–94.
20. Collins DL, Neelin P, Peters TM, et al. Automatic 3D intersubject registration of MR volumetric data in standardized Talairach space. *J Comput Assist Tomogr* 1994;18:192–205.
21. Sled JG, Zijdenbos AP, Evans AC. A nonparametric method for automatic correction of intensity nonuniformity in MRI data. *IEEE Trans Med Imaging* 1998;17:87–97.
22. Jones SE, Buchbinder BR, Aharon I. Three-dimensional mapping of cortical thickness using Laplace's equation. *Hum Brain Mapp* 2000;11:12–32.
23. Lee BC, Schmidt RE, Hatfield GA, et al. MRI of focal cortical dysplasia. *Neuroradiology* 1998;40:675–683.
24. Chan S, Chin SS, Nordli DR, et al. Prospective magnetic resonance imaging identification of focal cortical dysplasia, including the non-balloon cell subtype. *Ann Neurol* 1998;44:749–757.
25. Colombo N, Tassi L, Galli C, et al. Focal cortical dysplasias: MR imaging, histopathologic, and clinical correlations in surgically treated patients with epilepsy. *AJNR Am J Neuroradiol* 2003;24:724–733.
26. Avoli M, Bernasconi A, Mattia D, et al. Epileptiform discharges in the human dysplastic neocortex: in vitro physiology and pharmacology. *Ann Neurol* 1999;46:816–826.
27. Chassoux F, Devaux B, Landre E, et al. Stereoelectroencephalography in focal cortical dysplasia: a 3D approach to delineating the dysplastic cortex. *Brain* 2000;123:1733–1751.
28. Boonyapisit K, Najm I, Klem G, et al. Epileptogenicity of focal malformations due to abnormal cortical development: direct electrocorticographic-histopathologic correlations. *Epilepsia* 2003;44:69–76.
29. Palmini A, Andermann F, Olivier A, et al. Focal neuronal migration disorders and intractable partial epilepsy: a study of 30 patients. *Ann Neurol* 1991;30:741–749.